Cell Death and Differentiation (2010) 17, 1141–1154

www.nature.com/cdd

Type 3 inositol 1,4,5-trisphosphate receptor negatively regulates apoptosis during mouse embryonic stem cell differentiation

J Liang[1], Y-J Wang[1], Y Tang[1], N Cao[1], J Wang[1] and H-T Yang*[,1,2,3]

Ca^{2+} signals generated by inositol 1,4,5-trisphosphate receptors (IP_3Rs) are crucial for cellular processes such as apoptosis and differentiation. However, the exact roles of IP_3Rs and their contributions to Ca^{2+} signals in pluripotent embryonic stem (ES) cell behaviors remain largely unknown. In this study, we showed that the expression of type 3 IP_3R (IP_3R3) was transiently downregulated with a concomitant increase in apoptosis at the early differentiation stage of murine ES cells. Knockdown of IP_3R3 by small interfering RNA increased apoptosis in differentiating cells but not in undifferentiated ES cells. Moreover, IP_3R3 overexpression had the opposite effect. Consistently, IP_3R3 knockdown altered Ca^{2+} oscillations in differentiating cells but not in undifferentiated ES cells. The apoptosis in differentiating IP_3R3-knockdown cells was decreased by chelating intracellular Ca^{2+} with BAPTA-AM and increased in control ones. Furthermore, IP_3R3 knockdown led to a suppression of the expression of mesodermal and mesoendodermal but not ectodermal markers. The differentiation suppressions were further confirmed by the impaired differentiation of mesodermal and some of the endodermal but not ectodermal derivatives. Such defects were partially because of the increased apoptosis in Flk-1^+ cells. These findings provide the first demonstration of the important role of IP_3R3 in the regulation of apoptosis in early differentiating ES cells and subsequent lineage commitments through modulation of Ca^{2+} signals.

Cell Death and Differentiation (2010) **17,** 1141–1154; doi:10.1038/cdd.2009.209; published online 15 January 2010

Embryonic stem (ES) cells, derived from the inner cell mass of preimplantation embryo,[1,2] are pluripotent cells having the ability to differentiate into derivatives of all three germ layers (endoderm, mesoderm, and ectoderm) *in vitro*.[1,3] Such differentiation is concomitant with the reduction of proliferation and the occurrence of spontaneous apoptosis,[4,5] an essential process for the formation of cavities during embryogenesis *in vivo*.[6] Thus, ES cells recapitulating the early stages of lineage differentiation and spontaneous apoptosis represent an appropriate model to study the regulatory mechanisms underlying early embryogenesis.[7]

Intracellular Ca^{2+} oscillation has crucial roles in regulation of various cellular processes including proliferation,[8,9] differentiation,[10–12] and apoptosis.[8,13] Cells generate their Ca^{2+} signals by using both internal and external sources of Ca^{2+}. Inositol 1,4,5-trisphosphate receptors (IP_3Rs) are predominant intercellular Ca^{2+} release channels on the internal Ca^{2+} store endoplasmic reticulum (ER) and have important roles in the regulation of cellular behaviors through generation of spatially and temporally signal patterns of cytosolic free Ca^{2+} concentration ($[Ca^{2+}]_i$). Three days after withdrawal of leukemia inhibitory factor (LIF), approximately 30% of differentiated mouse (m) ES cells die by apoptosis.[5] Blocking this spontaneous apoptosis by a p38 mitogen-activated protein kinase inhibitor leads to an alteration of expression of differentiation markers and increased expression of the anti-apoptotic protein Bcl-2, Bcl-X_L, and Ca^{2+}-binding proteins,[14] indicating an important role of a correct apoptotic process in the regulation of ES cell differentiation and a possible role of Ca^{2+} signals in the regulation of apoptosis. Indeed, in many other cell types, such as lymphocytes or HEK293, Ca^{2+} signals regulated by IP_3Rs have been reported as a pro-apoptotic[13,15] or an anti-apoptotic mediator when anti-apoptotic factor Bcl-X_L is expressed.[16,17] However, the precise role of IP_3Rs in the regulation of apoptosis during early ES cell differentiation is unknown.

[1]Key Laboratory of Stem Cell Biology, Institute of Health Sciences, Shanghai Institutes for Biological Sciences (SIBS), Chinese Academy of Sciences (CAS) and Shanghai Jiao Tong University School of Medicine (SJTUSM), Shanghai, China; [2]Laboratory of Molecular Cardiology of Shanghai Stem Cell Institute, SJTUSM, Shanghai, China and [3]Shanghai Key Laboratory of Vascular Biology, Ruijin Hospital, SJTUSM, Shanghai, China
*Corresponding author: H-T Yang, Institute of Health Sciences, 225 Chong Qing Nan Road, Shanghai 200025, China. Tel/Fax: +86 21 63852593;
E-mail: htyang@sibs.ac.cn
Keywords: ES cells; IP_3R3; Ca^{2+} oscillation; apoptosis; proliferation
Abbreviations: AFP, α-fetoprotein; Alb1, albumin 1; ALP, alkaline phosphatase; αMHC, cardiac cytoskeletal proteins myosin heavy chain α; BAPTA-AM, 1,2-bis (2-aminophenoxy) ethane-*N,N,N′,N′*-tetraacetic acid-acetoxymethyl ester; BrdU, bromodeoxyuridine; $[Ca^{2+}]_i$, cytosolic free concentration; CK8, cytokeratin 8; Col2a1, collagen II; Dab-2, disabled-2; EBs, embryoid bodies; ER, endoplasmic reticulum; ES, embryonic stem; Gsc, goosecoid; GADPH, glyceraldehyde 3-phosphate dehydrogenase; HNF3β, hepatocyte nuclear factor 3 β; IP_3Rs, inositol 1,4,5-trisphosphate (IP_3) receptors; LIF, leukemia inhibitory factor; MAP2, microtubule-associated protein 2; MEF, mouse embryonic fibroblast; Mef2c, myocyte enhancer factor 2C; MLC-2v, myosin light chain-2v; MTT, 3-(4,5-dimethylthiazol-2-yl)-2,5-diphenyltetrazolium-bromide; NF-M, neurofilament; Nkx2.5, NK2 transcription factor; PE, phycoerythrin; PI, propidium iodide; PPARγ, peroxisome proliferator-activated γ; Q-PCR, quantitative RT-PCR; RNAi, RNA interference; siEGFP, EGFP-RNAi; sdc4, Syndecan-4; siIP_3R3, IP_3R3-siRNA; SSEA-1, stage-specific embryonic antigen 1; T, *brachyury*; Tuj1, class III-tubulin; TUNEL, terminal deoxynucleotidyltransferase-mediated dUTP-biotin nick end labeling; wt, wild type
Received 05.5.09; revised 17.11.09; accepted 30.11.09; Edited by V De Laurenzi; published online 15.1.10

There are three subtypes of IP_3Rs in mammalian cells, sharing high similarity (70–80%) in their primary sequences, but expressing to varying degrees in individual cell types and differing in molecular properties in many respects such as affinities for IP_3 and Ca^{2+}.[18,19] Type 1 IP_3R (IP_3R1) is predominantly expressed in brain tissue[20] and has a critical role in brain functions[21] and neural development.[22] The other two subtypes, type 2 and 3 IP_3R (IP_3R2 and IP_3R3), are expressed in various tissues and cell lines,[19] but their exact functions are difficult to assess because of their co-expression in tissues and the lack of selective inhibitors. Several pieces of evidence have shown that early embryonic development is disrupted by pharmacological[10,12] or antibody blockages[11] of IP_3Rs and phospholipase C, suggesting that IP_3-induced Ca^{2+} release is required for the early embryonic development in vertebrates. However, it is not clear to what extent the distinct IP_3R subtypes contribute to the complex Ca^{2+} signals during embryogenesis. Recent studies showed that the expression level of IP_3R3 increases after fertilization in zebrafish,[12] indicating a possible involvement of IP_3R3 in the regulation of Ca^{2+} signaling during early embryo development. IP_3R3 is also detected in mES cells[23,24] and it has been shown to mediate Ca^{2+} oscillations related to cell cycle regulation.[24] However, little is known regarding the exact function of IP_3R3 in undifferentiated and differentiating ES cells.

In this study, combining with specific RNA interference (small interfering RNA (siRNA)) and overexpression of IP_3R3, we analyzed the expression profile and roles of IP_3R3 during early differentiating mES cells. Our results have revealed novel roles of IP_3R3 in the regulation of intracellular Ca^{2+} oscillations and the biophysical functions in the apoptosis of early differentiating ES cells and the subsequent cell lineage commitment.

Results

Expression patterns of IP_3R3 in undifferentiated and differentiating ES cells. We first tested differentiating mES cell cultures for the expression profile of IP_3R3. As shown in Figure 1a, the expression of IP_3R3 mRNA and protein was higher in undifferentiated ES cells, while the expression levels decreased by 45% in mRNA and by 60% in protein at the first day of differentiation on withdrawal of LIF and feeder layers, and then gradually returned to the level observed in the undifferentiated ES cells around differentiation day 7, suggesting an important role of IP_3R3 during ES cell differentiation.

Characteristics of IP_3R3–siRNA ($siIP_3R3$) ES cell lines. To identify the role of IP_3R3, we then generated stable mES cell lines with downregulated expression of IP_3R3 by siRNA against IP_3R3 ($siIP_3R3a$, Figure 1b); RT-PCR and western blot analysis showed that the negative control siRNA against enhanced green fluorescent protein (siEGFP) did not affect the expression of three subtypes of IP_3Rs, while the $siIP_3R3a$ inhibited the expression of IP_3R3 but not IP_3R1 and IP_3R2. Compared with the wild-type (wt) or siEGFP ES cells, the expression of IP_3R3 in $siIP_3R3a$ mES cell lines (clones 4 and 2) was decreased by 40–50% at the RNA level (Figure 1c, left panel) and by 75–80% at the protein level (Figure 1c, right panel). During differentiation processes, the expression pattern of IP_3R3 in IP_3R3-knockdown cells (clones 2 and 4) was similar to that in control cells, although the expression levels at each time point examined were much lower than those of the control cells (Supplementary Figure 1).

To determine whether IP_3R3 regulates self-renewal, proliferation, and apoptosis in ES cells, we compared these characteristics between undifferentiated wt and $siIP_3R3a$ ES cells. No significant differences in the alkaline phosphatase (ALP) activity (Figure 2a) and in the transcripts of pluripotency markers Oct-4, Nanog, and Rex-1 (Figure 2b) were detected among undifferentiated wt, siEGFP, and $siIP_3R3a$ ES cells. Western blot and flow cytometry analysis further confirmed that the expression levels of pluripotency markers Oct-4 and stage-specific embryonic antigen 1 (SSEA-1) were similar among these cells (Figure 2c). In addition, MTT assay showed that undifferentiated $siIP_3R3a$ ES cells had similar cell viability as wt and siEGFP cells (Figure 3a, left panel). Taken together, these data suggest that IP_3R3 knockdown does not affect the self-renewal of ES cells.

IP_3R3 regulates apoptosis in differentiating ES cells. We then analyzed the roles of IP_3R3 during the spontaneous differentiation process. Compared with the wt and siEGFP ES cells, differentiating $siIP_3R3a$ ES cells had lower cell viability during examination on differentiation days 3 to 6 (Figure 3a, right panel). This was consistent with the decreased population of $siIP_3R3a$ ES cells observed on differentiation day 3 (Figure 3b). To determine the basis of this growth defect, we then analyzed the changes in proliferation and apoptosis in the differentiating cells. The numbers of bromodeoxyuridine (BrdU)-labeled cells in wt, siEGFP, and two $siIP_3R3a$ cell lines on differentiation day 3 were not significantly different when examined by confocal microscopy (Figure 3c) and flow cytometry analysis (Figure 3d). Flow cytometry analysis of each cell line on propidium iodide (PI) staining revealed no difference in cell cycle distribution among the cell lines, although the percentage of cells in $S–G_2–M$ stages gradually decreased on differentiation (Figure 3e). These data show that IP_3R3 downregulation decreases cell viability without affecting cell proliferation rates.

To determine whether the lower viability observed in the differentiating $siIP_3R3a$ ES cells is related to the increased apoptosis in early ES cell differentiation, we then compared apoptotic parameters among wt, siEGFP, and $siIP_3R3a$ ES cells. Annexin V (an early apoptosis marker)-FITC staining analysis showed similar apoptotic rates ($\sim$6%) among undifferentiated cell lines, while apoptotic cells increased in siEGFP cells at differentiation day 3 and further increased in both $siIP_3R3a$ cell lines compared with wt and siEGFP cells at differentiation day 3 (Figure 4a). Terminal deoxynucleotidyl-transferase-mediated dUTP-biotin nick end labeling (TUNEL) staining assay also showed that the $siIP_3R3a$ cells had up to twofold increases in apoptosis compared with the wt and siEGFP cells at differentiation day 3 (Figure 4b). The findings suggest that IP_3R3 downregulation does not affect the

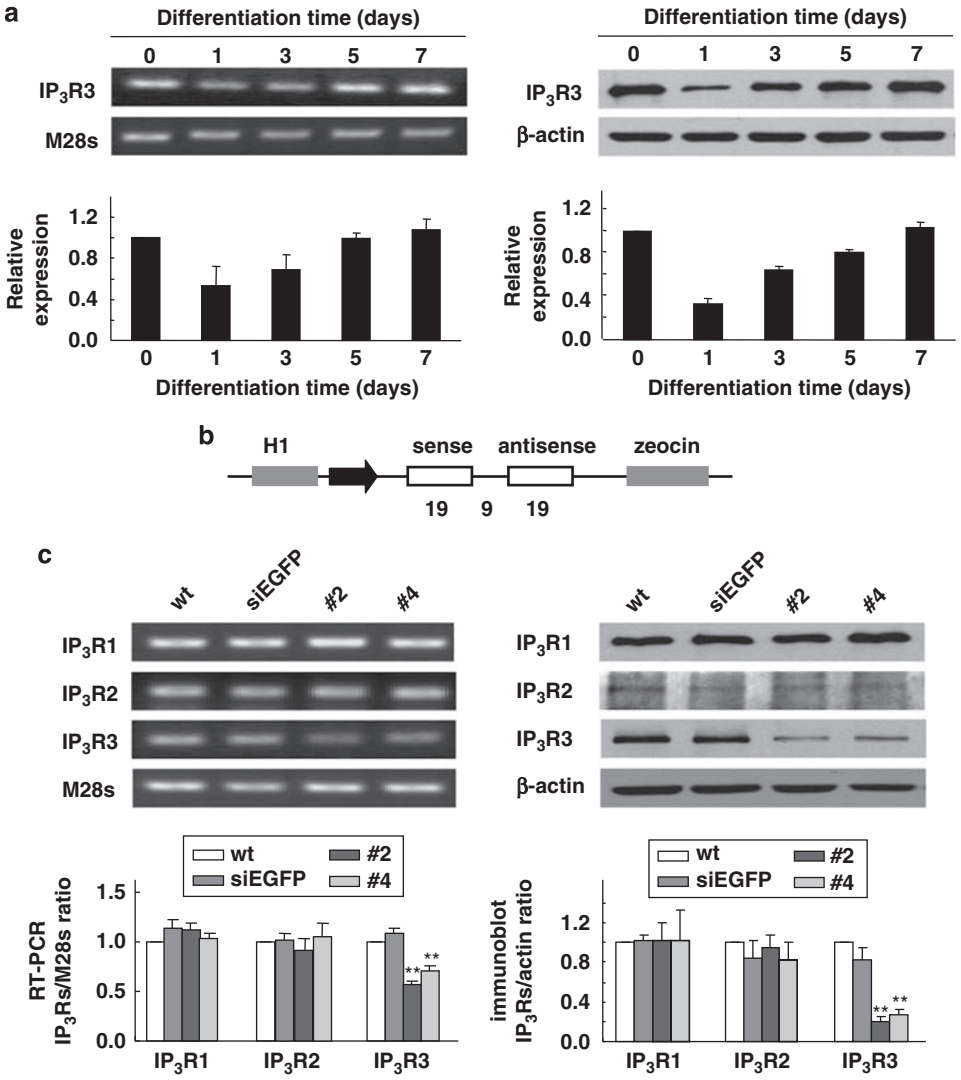

Figure 1 Specific downregulation of IP$_3$R3 in mES cells. (**a**) RT-PCR and western blot analysis of transcripts (left panel) and proteins (right panel) for IP$_3$R3 in undifferentiated and differentiating ES cells. (**b**) Schematic pTER$^+$ construction of RNA interference expression vectors for EGFP or IP$_3$R3. H1, promoter of polymerase III H1. (**c**) mRNA and protein expression of IP$_3$R isoforms in undifferentiated ES cells transfected with siEGFP or siIP$_3$R3a by RT-PCR (left panel) and western blot (right panel) analysis, respectively. #2 and #4, two siIP$_3$R3a ES cell clones. Lower panel, the averaged relative values derived from each clone were normalized against the endogenous standard gene *M28s* or β-actin. Data are represented as mean ± S.E.M. All experiments were repeated at least three times. $^{**}P<0.01$ compared with the corresponding control values

proliferation potential of differentiating ES cells, but it leads to an increase in apoptosis during differentiation, thereby conferring a growth defect on siIP$_3$R3a cells.

It has been shown that spontaneous apoptosis observed in differentiating mES cells is associated with the cleavage of caspase-3.[5,14] We thus evaluated caspase-3 activity by CaspACETM colorimetric assay system and western blot analysis. The siIP$_3$R3a cells had higher activities of caspase-3 (Figure 4c, left panel) as well as more total and cleaved caspase-3 proteins on differentiation day 3 (Figure 4c, right panel). The expression of other apoptotic marker proteins, Bax and *puma* α, and release of cytochrome *c*, the factors involved in mitochondrial apoptosis pathway, were also increased in siIP$_3$R3a cells on differentiation day 3 (Figure 4d).

To further confirm the role of IP$_3$R3 in the apoptosis of differentiating ES cells, we transiently transfected mES cells with another IP$_3$R3-specific siRNA (siIP$_3$R3b[25]) and wt IP$_3$R3-overexpressing vectors (IP$_3$R3wt) (Figure 4e). Consistent with the observation in siIP$_3$R3a cells, siIP$_3$R3b cells had more Annexin V$^+$ (Figure 4f) and TUNEL$^+$ cells (Figure 4g) compared with the control siEGFP cells on differentiation day 3. In contrast, the cells expressing IP$_3$R3wt (rat wt IP$_3$R3 inserted into pCB6 vector) had less apoptosis compared with the cells transfected with control pCB6 vector (Figures 4f and g).

Alteration of cytosolic Ca^{2+} signals generated by IP$_3$R3 knockdown leads to increased apoptosis. We further examined the mechanism of increased apoptosis in siIP$_3$R3

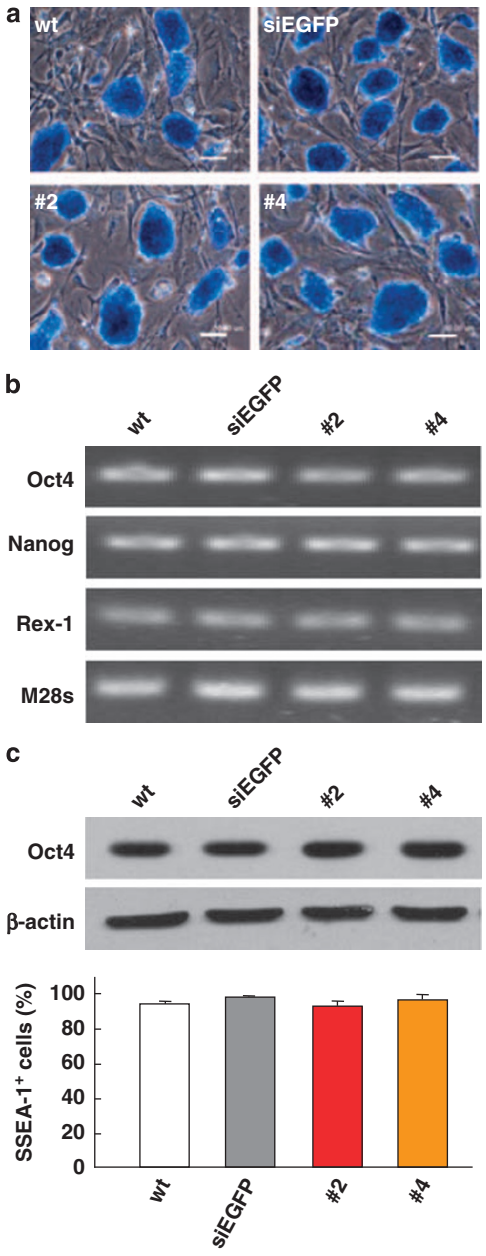

Figure 2 Characteristics of undifferentiated siIP$_3$R3 mES cells. (**a**) Photomicrographs and ALP staining of undifferentiated wt, siEGFP, siIP$_3$R3a clone 2 and 4 ES cells. (**b**) Analysis of pluripotency markers Oct-4, Nanog, and Rex-1 by RT-PCR. (**c**) Western blot analysis of Oct-4 expression (upper panel) and flow cytometry analysis of SSEA1 epitope expression in undifferentiated wt, siEGFP, siIP$_3$R3a clone 2 and 4 ES cells. Percentages of SSEA1-positive cells per sample resulted from analysis of 10 000 events. Data are represented as mean ± S.E.M. All experiments were repeated at least three times

cells. As IP$_3$Rs is a Ca^{2+} release channel on ER and other intracellular organelles,[19] we measured spontaneous $[Ca^{2+}]_i$ oscillations in undifferentiated and differentiating ES cells. The $[Ca^{2+}]_i$ oscillation patterns were similar between siEGFP control and siIP$_3$R3a undifferentiated ES cells (Supplementary Figure 2). However, the Ca^{2+} signal patterns were markedly different between the control and siIP$_3$R3a differentiating cells. In control cells, Ca^{2+} oscillations were sharp with lower frequency (Figure 5b, left panel), whereas siIP$_3$R3a cells showed much more robust and long-lasting Ca^{2+} oscillations with higher baseline $[Ca^{2+}]_i$ (Figures 5a and b, right panel). The averaged baseline, incidence, and intensity of $[Ca^{2+}]_i$ oscillations in siIP$_3$R3a cells were much higher than those of control cells (Figure 5b). These data suggest that IP$_3$R3 has an important role in maintaining a proper pattern of cytosolic Ca^{2+} signals in early differentiating cells.

To further determine whether IP$_3$R3 knockdown-increased $[Ca^{2+}]_i$ oscillations would promote apoptosis, we examined the apoptosis of differentiating ES cells after chelating cytosolic free Ca^{2+} by addition of 1,2-bis (2-aminophenoxy) ethane-*N,N,N′,N′*-tetraacetic acid-acetoxymethyl ester (BAPTA-AM). BAPTA-AM decreased the total and cleaved caspase-3 in a dose-dependent manner in siIP$_3$R3a cells, whereas it increased cleaved caspase-3 in siEGFP cells on differentiation day 3 (Figure 5c). Consistently, BAPTA-AM treatment decreased TUNEL-positive cells in differentiating siIP$_3$R3 cells, whereas it increased TUNEL-positive cells in siEGFP cells (Figure 5d). These findings suggest that cytosolic Ca^{2+} signals regulated by IP$_3$R3 might have crucial roles in the regulation of apoptosis during mES cell differentiation.

Knockdown of IP$_3$R3 impairs *in vitro* differentiation of the mesoderm and endoderm. To analyze whether IP$_3$R3 also affects lineage-specific differentiation, the siIP$_3$R3a cells were induced to differentiate into three primary germ layers and their derivatives by the formation of embryoid bodies (EBs). The EBs formed from siIP$_3$R3a cells were smaller than those formed from wt or siEGFP cells after 2-day hanging drop culture (Figure 6a, day 2). However, after suspension culture for another 4 days, the siIP$_3$R3a EBs swelled and became much larger than the control ones (Figure 6a, day 6). The Q-PCR analysis showed that the expression of undifferentiated marker genes *Oct-4* and *Rex-1* gradually decreased during ES cell differentiation, but without difference among the wt, siEGFP, and two siIP$_3$R3a cell lines (Figure 6b). It is noteworthy that the expression patterns of early endodermal markers Gata4 and Gata6, and ectodermal markers Fgf5 and nestin in siIP$_3$R3a cells were similar to those in wt and siEGFP ES cells (Figure 6b). However, the expressions of early mesodermal or mesendodermal markers *brachyury* (T), goosecoid (Gsc), Flk1, and Hand1 were much lower in siIP$_3$R3a cells than in control cells in the indicated days (Figure 6c).

Next, we compared the *in vitro* differentiation of neuronal cells (ectoderm), cardiomyocytes, adipocytes, and cartilage cells (mesoderm), and endodermal cell types from wt, siEGFP, and two lines of siIP$_3$R3 cells. The expression of neuronal-specific markers[26] microtubule-associated protein 2 (MAP2) as well as class III-tubulin (Tuj1) and neurofilament genes (NF-M) remained unchanged after IP$_3$R3 knockdown (Supplementary Figure 3a). It was further confirmed by immunofluorescence analysis of MAP2 and Tuj1 that down-regulation of IP$_3$R3 did not affect the neuronal differentiation (Supplementary Figure 3b).

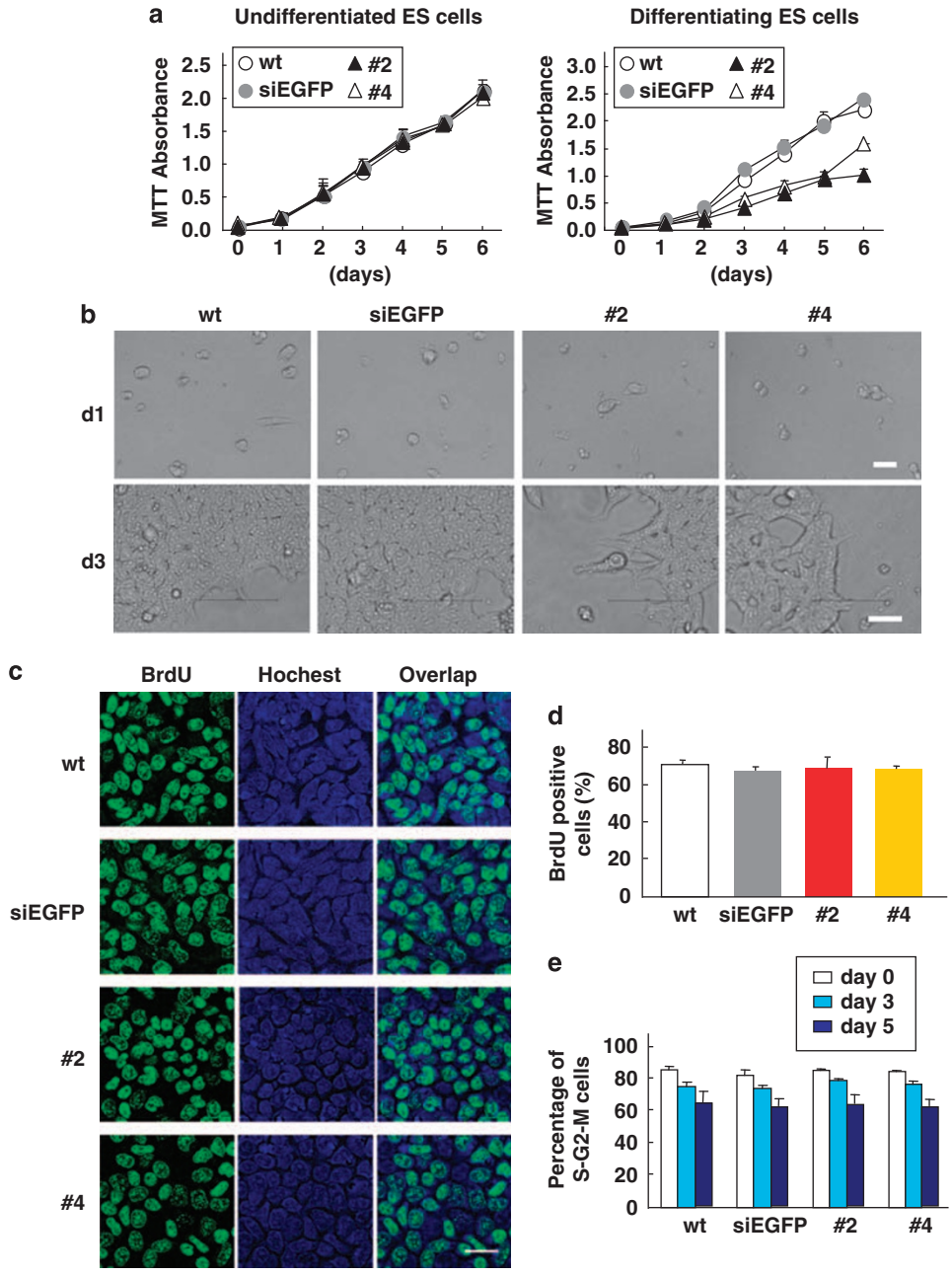

Figure 3 Differentiating siIP$_3$R3 ES cells show a proliferative defect. (**a**) Proliferation rates of undifferentiated and differentiating wt, siEGFP, siIP$_3$R3a clone 2 and 4 ES cells analyzed by MTT assays for 6 consecutive days. (**b**) The morphology of control and siIP$_3$R3a cells was monitored by microscopy on differentiation days 1 and 3. Bars = 50 μm. (**c**) Immunohistochemical detection of BrdU incorporation in ES cells after a 3-day differentiation. Cellular incorporation of BrdU during S phase was detected with an anti-BrdU antibody (green). Nuclei were counterstained with Hochest 33342 (blue). Bars = 50 μm. (**d**) Flow cytometric analysis of BrdU incorporation in day 3 differentiated ES cells. (**e**) Analysis of cell cycle distribution by PI staining and flow cytometry on differentiation days 0, 3 and 5. Data are represented as mean ± S.E.M. from at least three independent experiments

As expected, the percentage of contracting EBs (characteristics of cardiomyocytes) was much lower in IP$_3$R3-knockdown cells than in wt and siEGFP cells (Figure 7a). Similarly, the expressions of genes encoding the early cardiac transcription factors myocyte enhancer factor 2C (Mef2c) and NK2 transcription factor (Nkx2.5) as well as cardiac cytoskeletal proteins myosin heavy chain α (αMHC) and myosin light chain-2v (MLC-2v) were significantly lower in siIP$_3$R3a cells compared with those in control cells (Figure 7b). The immunofluorescence analysis confirmed much higher expression levels of cardiac cytoskeletal protein α-actinin and MLC-2v in wt and siEGFP EBs than in the siIP$_3$R3a ones (Figure 7c). In addition, to determine whether siIP$_3$R3 ES cells can differentiate into Flk1$^-$ mesodermal lineages other than cardiomyocytes from Flk1$^+$ mesodermal lineages, ES cells were induced to differentiate into adipogenic or chondrogenic lineage from Flk1$^-$ mesodermal lineages.[27] Alican blue-positive cartilage cells

(Supplementary Figure 4a, upper panel) or Oil red O-positive adipogenic cells (Supplementary Figure 4a, lower panel) were observed on differentiation day 21 in both types of cells. However, chondrogenic and adipogenic differentiation was less efficient in siIP$_3$R3 cells compared with that in control cells. Consistently, the expression of chondrogenic marker

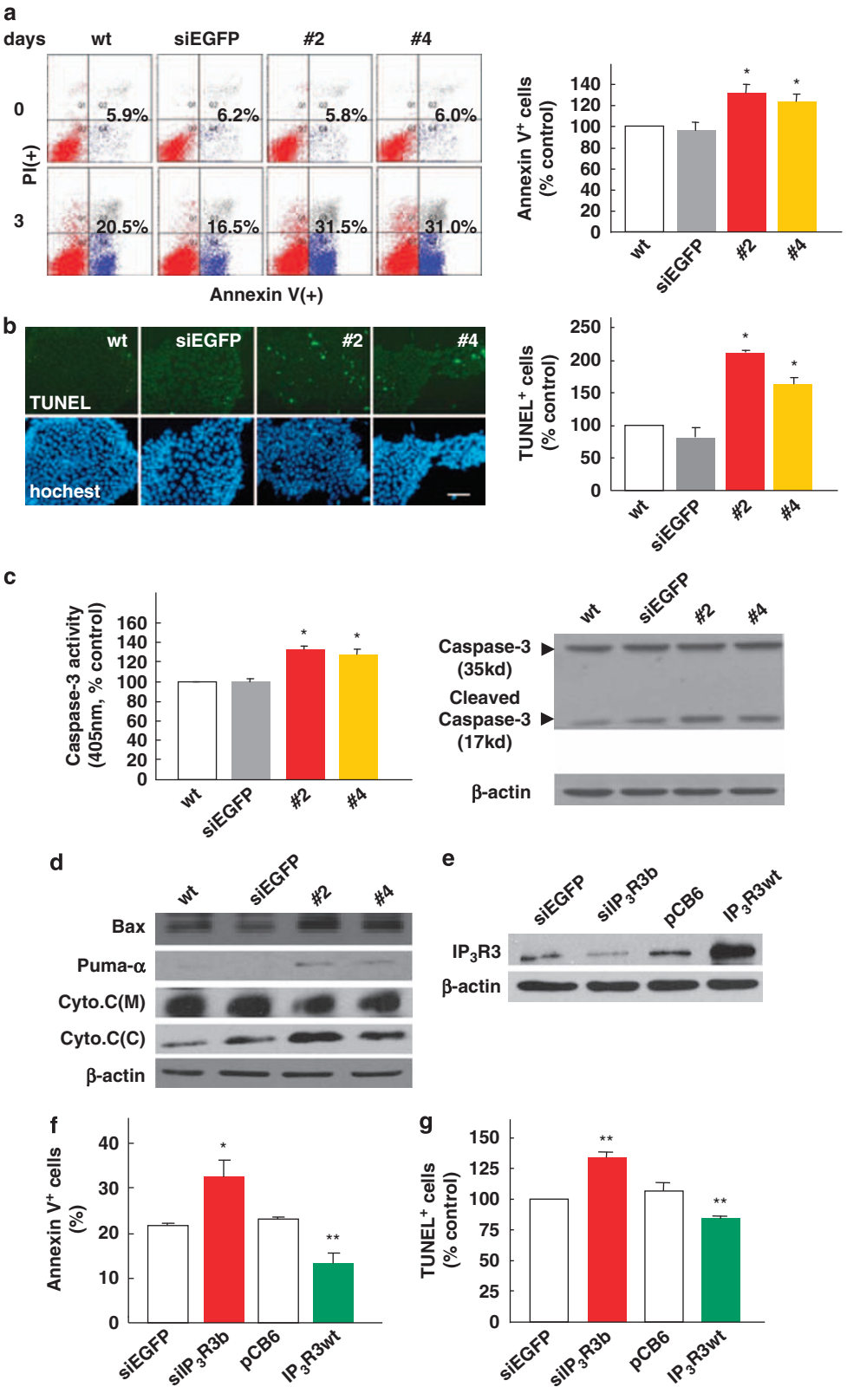

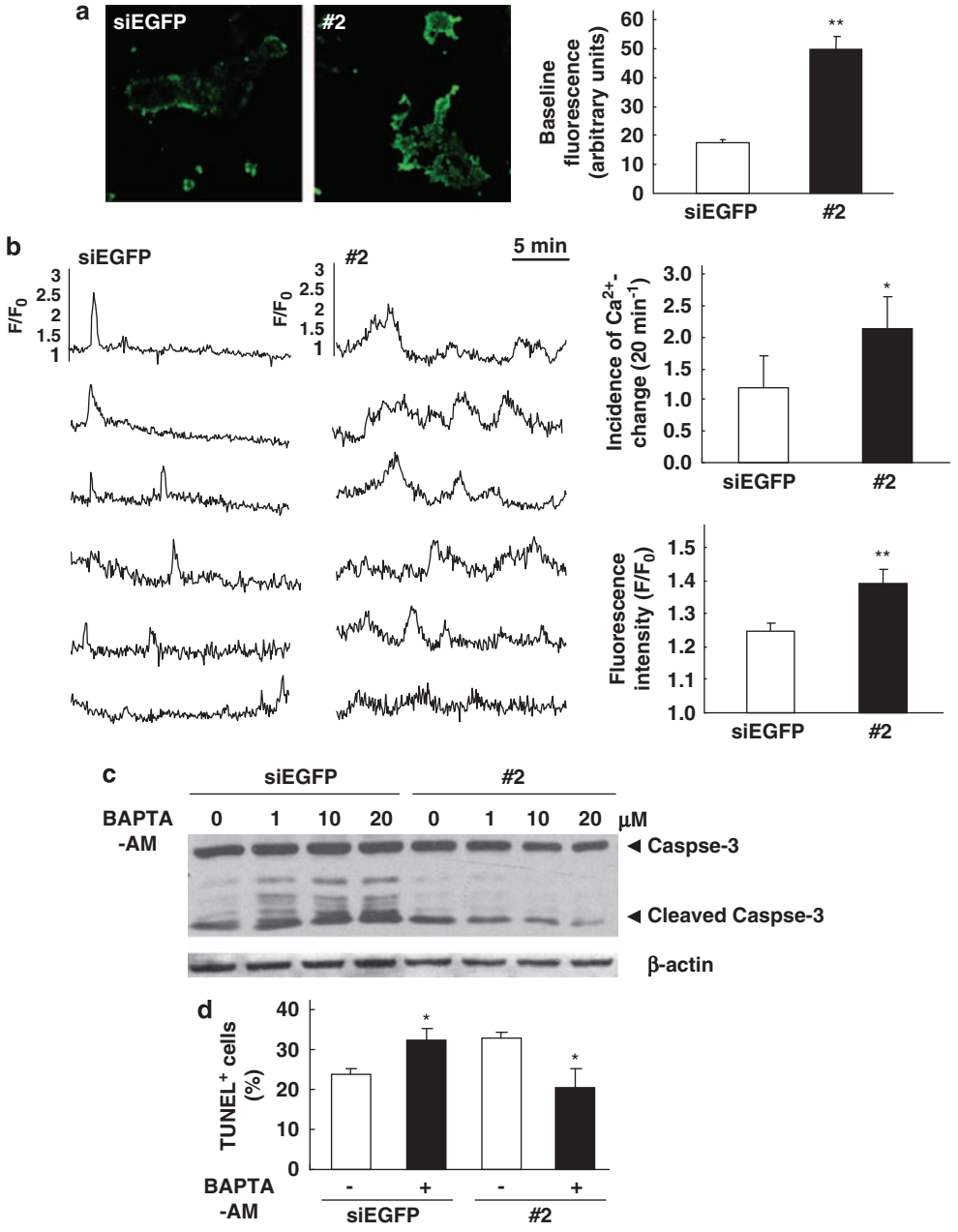

Figure 5 Elevation of Ca^{2+} signal generated by knockdown of IP$_3$R3 leads to increased apoptosis in differentiating ES cells. (**a**) Representative images (left panel) and averaged baseline fluorescence (right panel) of $[Ca^{2+}]_i$ oscillations in day 3 differentiating siEGFP and siIP$_3$R3a ES cells loaded with Ca^{2+} sensitive dye Fluo-4/AM. (**b**) Representative traces (left panel) and averaged incidence as well as intensity (right panel) of $[Ca^{2+}]_i$ oscillations detected by using two-dimensional confocal images taken at 5 s intervals from day 3 differentiating siEGFP and siIP$_3$R3a ES cells. (**c**) Western blot analysis of caspase-3 for the day 3 differentiating siEGFP and siIP$_3$R3a cells with or without treatment of Ca^{2+} chelator BAPTA-AM at various concentrations. (**d**) TUNEL staining analysis of apoptotic cells in day 3 differentiating siEGFP and siIP$_3$R3a cells with or without treatment of 20 μm BAPTA-AM. Data are represented as mean ± S.E.M. from at least three independent experiments. *$P<0.05$, **$P<0.01$ compared with the corresponding control values

Figure 4 IP$_3$R3 regulates apoptosis in differentiating ES cells. (**a**) Annexin V (*x* axis) and PI (*y* axis) staining of undifferentiated (day 0) and differentiating (day 3) wt, siEGFP, siIP$_3$R3a clone 2 and 4 ES cells. The numbers shown in each quadrant represent the percentage of cells staining positive for Annexin V but negative for PI (blue, left panel). The normalized data are shown in the right panel. (**b**) Immunohistochemical detection of apoptotic response in day 3 differentiating ES cells based on TUNEL analysis (left panel) and TUNEL-positive cells were quantified by flow cytometry analysis (right panel). Nuclei were counterstained with Hochest 33342. Bar = 10 μm. (**c**) Caspase-3 activity (left panel) and Western blot analysis of caspase-3 in day 3 differentiating ES cells. (**d**) Western blot analysis of Bax and *puma* α expressions as well as cytochrome *c* in the mitochondrial (M) and cytosolic (C) fractions in day 3 differentiating ES cells. β-Actin was used as a loading control. (**e**) Western blot analysis of IP$_3$R3 in cells after being transiently transfected with siEGFP, siIP$_3$R3b (another specific siRNA for IP$_3$R3), control pCB6, and pCB6-IP$_3$R3 (IP$_3$R3wt, upper panel). (**f**, **g**) Apoptotic cells were quantified by Annexin V (**f**) and TUNEL (**g**) staining followed by flow cytometry analysis in siEGFP, siIP$_3$R3b, control pCB6, and IP$_3$R3wt cells. Data are represented as mean ± S.E.M. from at least three independent experiments. *$P<0.05$, **$P<0.01$ compared with the corresponding control values

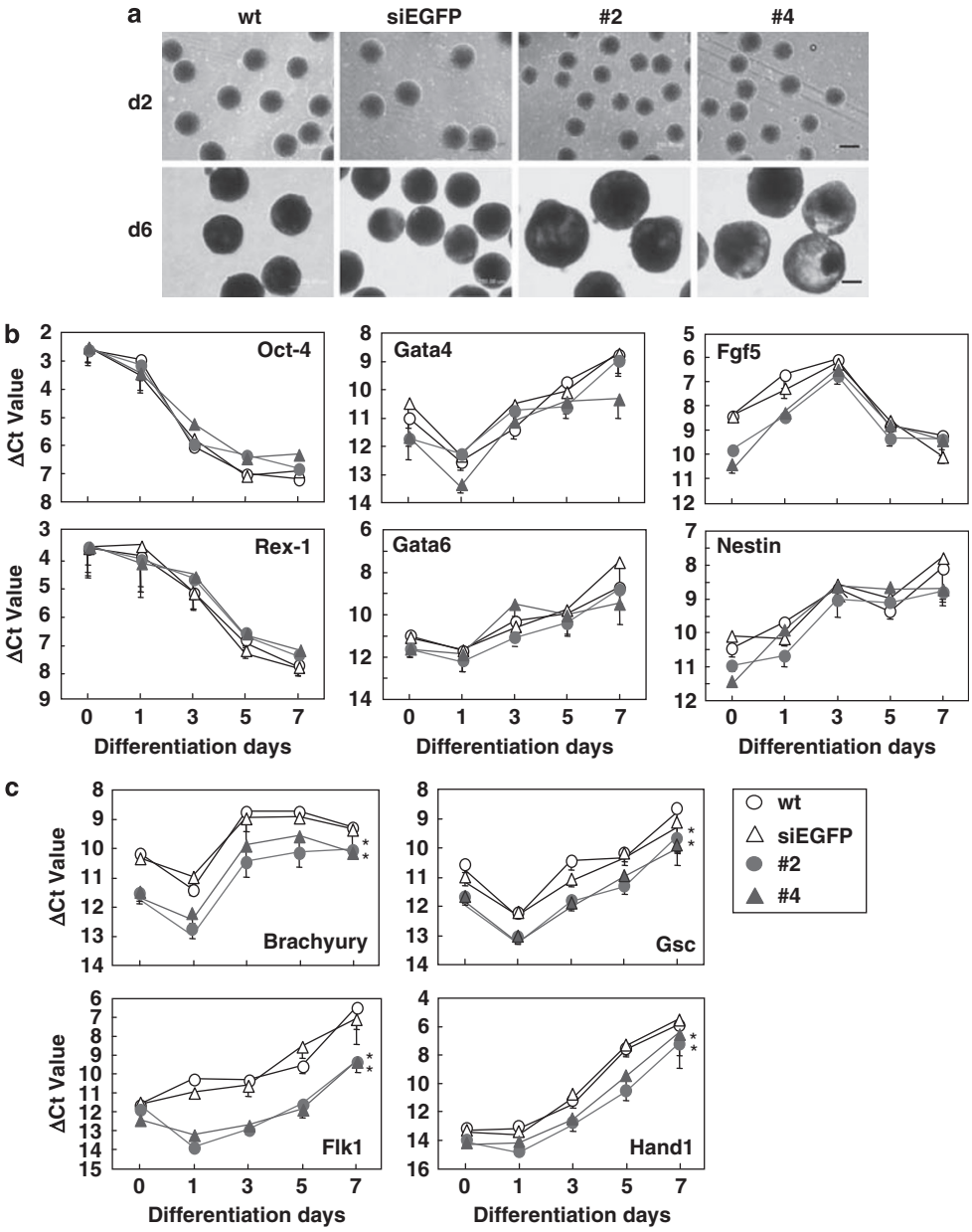

Figure 6 IP$_3$R3 knockdown represses early mesodermal and mesendodermal markers. (**a**) Embryoid body (EB) formation of wt, siEGFP, siIP$_3$R3a clone 2 and 4 ES cells on day 2 and day 6 of hanging drop differentiation. Bars = 250 μm. (**b**, **c**) Quantitative expression analysis of early differentiation markers Fgf5 and Nestin (ectoderm); Gata4 and Gata6 (endoderm); Brachyury, Gsc, Flk1, and Hand1 (mesoderm/mesendoderm); and the pluripotency markers Oct-4 and Rex-1 during ES differentiation. Ct values of Q-PCR analysis were normalized against GADPH. Data are represented as mean ± S.E.M. from at least three independent experiments. *$P<0.05$ compared with the corresponding wt group

genes *sox9*[28] and *collagen II*[29] (*Col2a1*) (Supplementary Figure 4b, left panel) and adipogenic marker genes *peroxisome proliferator-activated* γ (*PPAR*γ) and *adiponectin*[30] (Supplementary Figure 4b, right panel) was much lower in siIP$_3$R3 cells compared with that in control cells. Thus, downregulation of IP$_3$R3 affects the expression of early mesodermal markers and the subsequent differentiation of mesodermal lineages.

For endodermal differentiation, we examined the expression of hepatic cell marker genes[26] *cytokeratin 8* (*CK8*), *hepatocyte nuclear factor 3* β (*HNF3*β), α-*fetoprotein*, and *albumin 1* (*AlB1*) (Figure 7d, left panel) as well as visceral endodermal markers *Syndecan-4*[31] (*sdc4*), *tmpress2*,[32] and *disabled-2*[33] (*Dab-2*) (Figure 7d, right panel). The mRNA levels of AFP, AlB1, and Dab-2 decreased in siIP$_3$R3 cells compared with those in wt and siEGFP cells, whereas the expressions of CK8, HNF3β, sdc4, and tmpress2 remained unchanged (Figure 7d). The decreased protein expressions of AFP and Dab2 were further confirmed by immunofluorescence analysis (Figure 7e). Taken together, these data

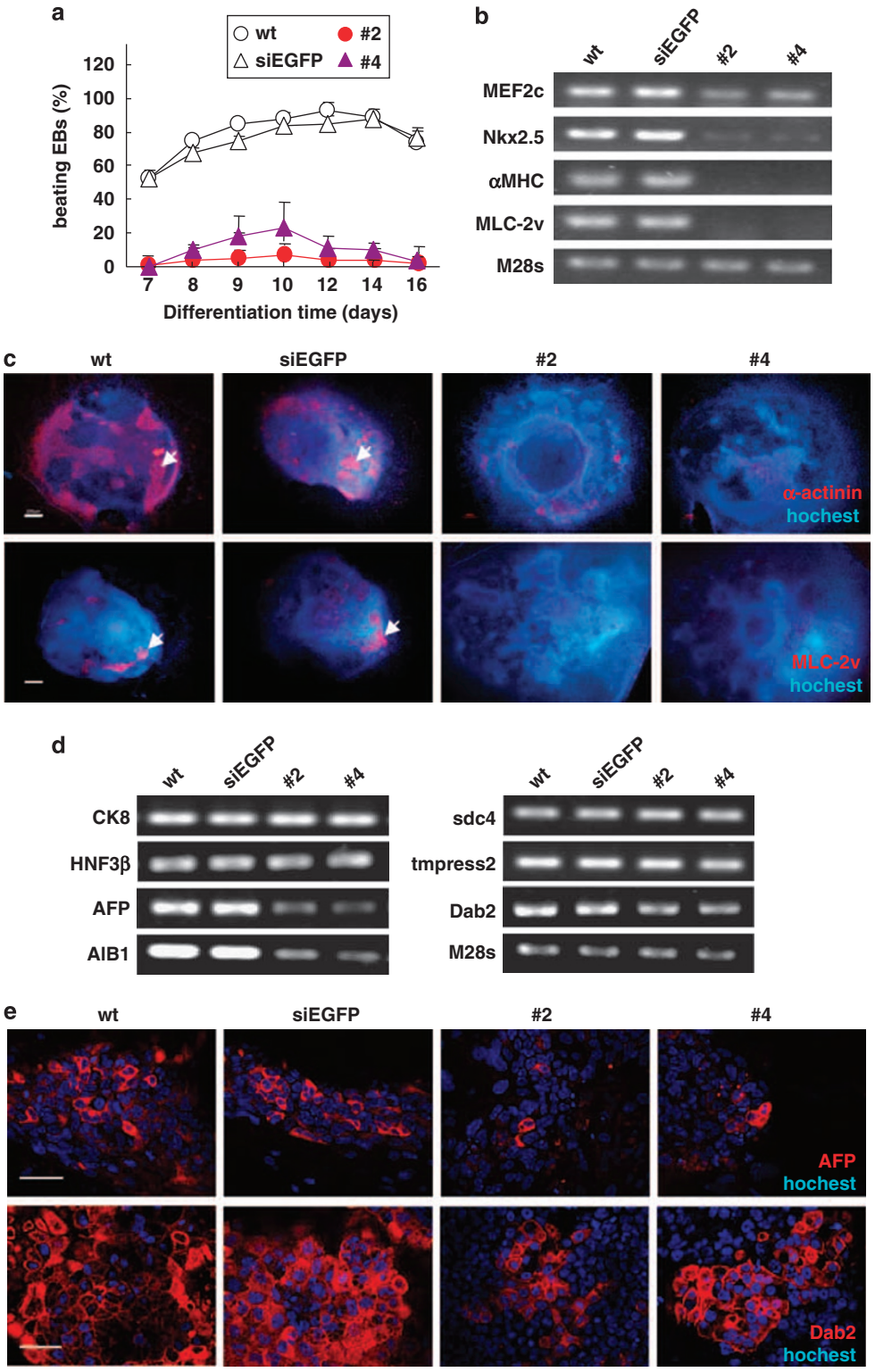

Figure 7 Cardiac and endodermal cell differentiation of wt, siEGFP, and siIP_3R3 ES cells. (**a**) Differentiation profile of cardiomyocytes during EB outgrowth. EBs, derived from different ES clones, were plated (day 7) and checked for beating clusters during differentiation days 7 to 16. RT-PCR analysis of wt, siEGFP, siIP_3R3a clone 2 and 4 ES cells for expressions of cardiac markers (**b**) at differentiation day 10 and definitive endodermal (**d**, left panel) as well as visceral endodermal (**d**, right panel) markers at differentiation day 14. Immunofluorescence analysis of α-sarcomeric actinin and MLC-2v in day 10 EBs (**c**, Bar = 200 μm) and endodermal markers AFP and Dab2 in day 14 EBs (**e**, Bar = 50 μm). The areas indicated by arrows show positive signals of cardiomyocyte. Data are represented as mean ± S.E.M. from at least three independent experiments

indicate that downregulation of IP$_3$R3 appears to affect mesodermal and some of the endodermal differentiation, but not ectodermal differentiation.

Relationship between the increased apoptosis and the differentiation defect in IP$_3$R3 knockdown cells. As shown above, the increased apoptosis is accompanied by defected mesodermal and endodermal differentiation with the IP$_3$R3 knockdown. Next, we examined whether the IP$_3$R3-knockdown-caused differentiation defect is due to the increased apoptosis. As the size of EBs could affect ES cell differentiation,[34] we therefore increased the initial cell numbers from 600 to 800 cells/20 μl in hanging drop stage to match the size of siIP$_3$R3a EBs with that of the control ones (Figure 8a). However, siIP$_3$R3a EBs at an initial density of 800 cells/20 μl still had a lower percentage of cardiomyocyte differentiation compared with the control siEGFP cells at an initial density of 600 cells/20 μl (Figure 8b), suggesting that the increased apoptosis observed in IP$_3$R3 cells may not occur evenly in all differentiating cells but rather in certain cell lineages, such as progenitors of mesoderm-derived cells. To analyze this possibility, we doubly stained early mesodermal marker Flk-1 and early apoptotic marker Annexin V and analyzed by flow cytometry in differentiating cells on day 3. Approximately 7.8% Flk-1$^+$ cells were detected in control cells, whereas only 2.3% Flk-1$^+$ cells were detected in siIP$_3$R3a cells (Figure 8c), a consistent result with the suppressed Flk-1 expression observed in Figure 6c. Meanwhile, in the Flk-1$^+$ control cells, a majority (69%) of the cells were Annexin V$^-$, whereas in Flk-1$^+$ siIP$_3$R3 cells,

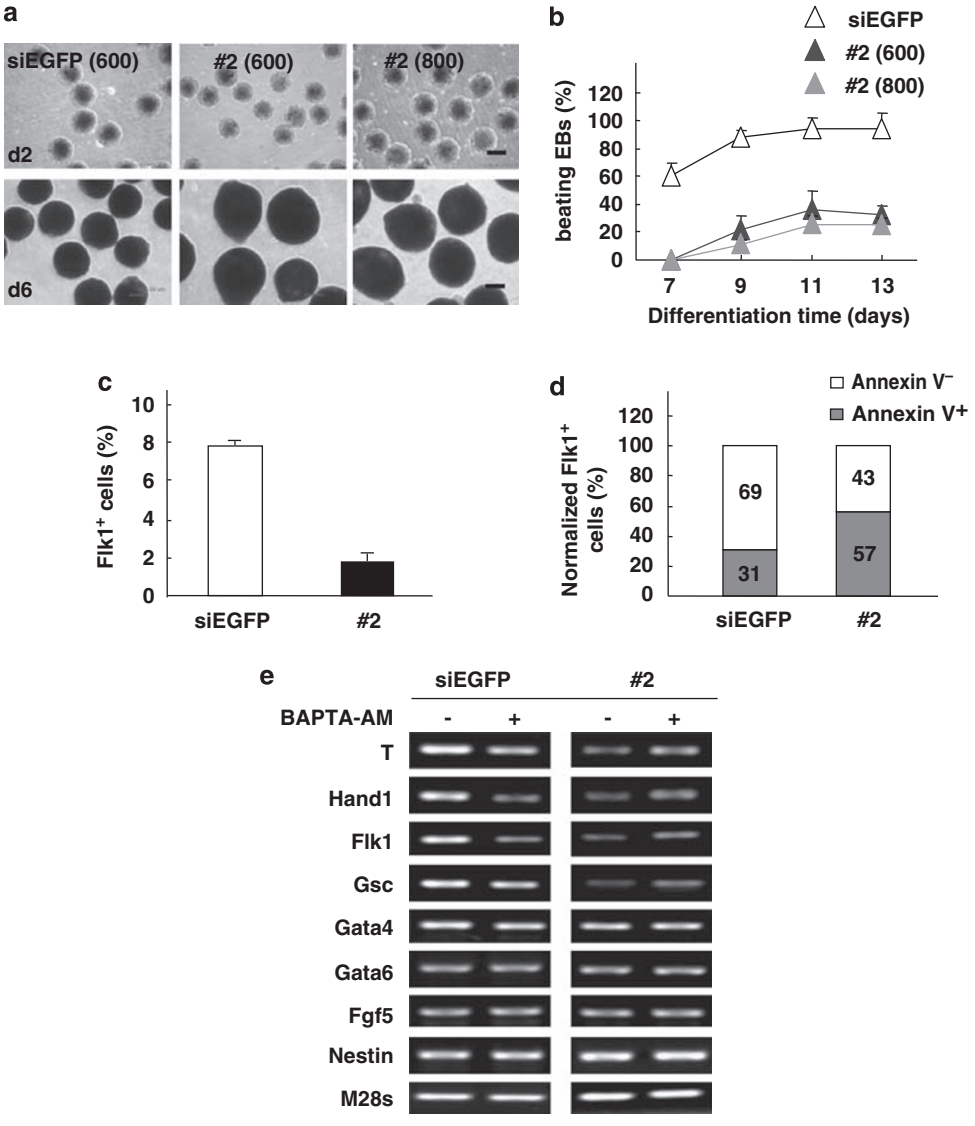

Figure 8 Relationship of increased apoptosis with the differentiation defect in IP$_3$R3 downregulation cells. (**a**) Embryoid body (EB) formation of siEGFP and siIP$_3$R3a ES cells at concentrations of 600 or 800 cells/20 μl on day 2 (upper panel) and day 6 (lower panel) of hanging drop differentiation. Bar = 250 μm. (**b**) Differentiation profile of cardiomyocytes during EB outgrowth. EBs were derived from different ES clones at an initial cell density of 600 or 800 cells/20 μl. (**c**, **d**) Cells were immuno-stained with Flk-1 (**c**) or double stained with Flk-1/Annexin V (**d**) and analyzed by flow cytometric assay on differentiation day 3. (**e**) RT-PCR analysis of early differentiation markers for day 3 differentiating siEGFP and siIP$_3$R3a cells with or without BAPTA-AM (10 μM) treatment

over 50% of the cells were Annexin V^+ (Figure 8d). The data suggest that more Flk-1^+ cells tend to undergo apoptosis after downregulation of IP_3R3. As IP_3R3 downregulation-enhanced apoptosis is prevented by the Ca^{2+} chelator BAPTA-AM, we further analyzed whether it could rescue the expression of mesodermal and mesendodermal markers in siIP_3R3 cells. As shown in Figure 8e, after the addition of BAPTA-AM, the expression of mesodermal and mesendodermal markers was rescued in siIP_3R3 cells but suppressed in control cells, whereas the expression of ectodermal and endodermal markers examined remained unchanged in both cell types. These data were consistent with the observation of BAPTA-AM-dependent alteration of apoptosis (Figures 5c and d), and suggest that IP_3R3 downregulation-increased apoptosis at least partially contributes to the subsequent suppression of mesodermal and mesendodermal differentiation.

Discussion

The release of intracellular Ca^{2+} through either IP_3Rs or ryanodine receptors (RyRs) activates a wide variety of signaling pathways in virtually every type of cell.[8,9] Generally, IP_3Rs are main intracellular Ca^{2+} channels in non-excitable cells, while RyRs contribute to internal Ca^{2+} release in excitable cells, such as cardiac and neuronal cells.[35] Consistently, as non-excitable cells, undifferentiated ES cells express three subtypes of IP_3Rs (Figure 1c) but not RyRs.[23,36] However, little is known regarding the specific function of each IP_3R subtype in the self-renewal and differentiation of ES cells. Here, we revealed the novel roles of IP_3R3 in the regulation of apoptosis of differentiating mES cells and cell lineage commitment. We also showed a relatively higher expression of IP_3R3 in undifferentiated ES cells, but IP_3R3 knockdown does not affect the characteristics of these cells. Although IP_3Rs-mediated Ca^{2+} oscillations are involved in cell cycle progression through G_1/S phases in mES cells based on the pharmacological interference,[24] alterations of Ca^{2+} oscillations by IP_3R3 knockdown are only observed in differentiating but not undifferentiated ES cells. This observation is consistent with the unchanged apoptosis and self-renewal properties of these cells. These results indicate that the contributory roles of IP_3R3 in mediating Ca^{2+} oscillations differ between undifferentiated and differentiating ES cells. The exact mechanism responsible for this discrepancy needs to be clarified in future.

One important finding of this study is the negative regulation of apoptosis by IP_3R3 during the early differentiation stage of ES cells. This effect seems to be associated with the alternation of Ca^{2+} signals as the increased apoptosis is accompanied by elevated Ca^{2+} signals in differentiating cells with IP_3R3 knockdown. In addition, chelating cytosolic Ca^{2+} signals by BAPTA-AM decreases the cleavage of caspase-3 and apoptosis in siIP_3R3 cells (Figure 5). These findings are consistent with the previous observation that elevated cytosolic Ca^{2+} signaling could lead to apoptotic responses by triggering an elevated mitochondrial matrix Ca^{2+} concentration, and thereby enable the release of apoptotic signaling molecules, such as cytochrome *c*,[25] and activate the caspases.[25,37] Indeed, we also found that the increased apoptosis by IP_3R3 knockdown is accompanied by increases in Bax expression, caspase-3 activity, and the release of cytochrome *c*, suggesting that a mitochondrial apoptosis pathway might be involved in this process. Additional experiments need to be performed to determine this possibility. However, how can IP_3R3 function as an anti-Ca^{2+} oscillatory factor in differentiating ES cells? A similar observation was obtained previously in Hela, COS-7, and CHO cells.[15,38] One of the interpretations is that IP_3R3 might have a negative feedback on the activation of other IP_3R subtypes because of its property of lacking the feedback inhibition by high $[Ca^{2+}]_i$,[38,39] while IP_3R1 and IP_3R2 are regulated by cytosolic Ca^{2+} in a biphasic manner;[40] however, a discrepancy remains.[41] In other words, the continuously releasing Ca^{2+} from IP_3R3 assures high $[Ca^{2+}]_i$ in an area surrounding other IP_3R subtypes and keeps them in an inactivated state, thereby terminating the cytosolic high $[Ca^{2+}]_i$. The precise roles of other IP_3R subtypes in the regulation of $[Ca^{2+}]_i$ and apoptosis, and the functional interaction among the IP_3Rs in differentiating ES cells need to be determined. IP_3R3 might also have an anti-Ca^{2+} oscillatory role through a negative feedback on plasma-membrane channels, such as the canonical transient receptor potential channel that is bound and regulated by IP_3R3.[42] In any case, it appears that IP_3R3 functions as an important regulator of other Ca^{2+} channels to maintain proper cytosolic Ca^{2+} signals. In addition, the Ca^{2+} oscillation patterns in differentiating control cells differ from those in siIP_3R3 cells (Figure 5b). The observation of increased apoptosis in control cells after chelating Ca^{2+} by BAPTA suggests that the Ca^{2+} signals in control cells may be responsible for apoptosis protection. In agreement with our results, the similar pattern of $(Ca^{2+})_i$ signals observed in the control cells has been shown to confer apoptosis resistance.[17] As differential Ca^{2+} signals, including the signal initiation, the amplitude and frequency of Ca^{2+} signals, as well as the duration of the Ca^{2+} elevation, may lead to different biological effects,[43] the different Ca^{2+} signals chelated by BAPTA in control and IP_3R3-knockdown cells may have opposite roles in the regulation of apoptosis. More detailed studies are needed to clarify these possibilities.

IP_3R3 appears to participate actively in apoptosis in a diversity of cell types, but its role in apoptosis is rather controversial. It has been shown that IP_3R3 preferentially mediates apoptosis in some lymphocytes and CHO cells,[13,15,44] whereas it increases cellular apoptotic resistance in the presence of anti-apoptotic factor Bcl-X_L in DT40 cells.[16,17] Therefore, the functional regulation of IP_3R3 in apoptosis may be dependent on the different modulators of IP_3Rs in the individual cells. It is noteworthy that the expression profile of Bcl-X_L is extremely similar to that of IP_3R3 (Supplementary Figure 5). It would be anticipated, therefore, that the relatively higher expression levels of Bcl-X_L and IP_3R3 in undifferentiated ES cells have an anti-apoptotic effect, while the lower expression levels of Bcl-X_L and IP_3R3 sensitize mES cells to apoptotic insults during the early differentiation stage. Future studies are needed to elucidate the regulation of Bcl-X_L on IP_3R3 in differentiating ES cells.

Consistent with the previous reports,[5,14] the apoptosis on differentiation day 3 increases compared with that of undifferentiated ES cells. The increased apoptosis observed

in IP_3R3 knockdown differentiating cells is accompanied by the lower expression of early mesodermal and mesendodermal markers but not early endodermal and ectodermal markers. Such lineage defection may be due to the increased apoptosis caused by IP_3R3 knockdown or due to a direct role of IP_3R3 on the differentiation other than apoptosis, or both. We found that the BAPTA-enhanced apoptosis in control cells is accompanied by the downregulation of expressions of mesodermal and mesendodermal markers. Consistently, the suppression of apoptosis by BAPTA in siIP_3R3 cells is accompanied by the rescue of these markers (Figure 8e). These results suggest a correlation between the apoptosis and mesodermal and mesendodermal differentiation. This hypothesis is supported by the observation that the proportion of early apoptotic cells (Annexin V^+) increases in Flk-1^+ (the early mesodermal marker[27]) cells after IP_3R3 knockdown. Taken together, these data suggest that the lower expression of early mesodermal markers and defected differentiation of mesodermal derivatives are at least partially because of the increased apoptosis in siIP_3R3 cells. In addition, the siIP_3R3 ES cells have defects in differentiation of some of the endodermal derivatives, in spite of the expression of analyzed early markers of the endoderm remaining unchanged. This might be due to the loss of some mesendodermal progenitors, such as Gsc^+ cells, because these cells could further differentiate into definitive endodermal derivatives.[45] Another probability is that IP_3R3 may have a direct effect on the later differentiation of endodermal derivatives. These possibilities need to be analyzed further. Interestingly, the roles of IP_3R3 in the regulation of apoptosis and differentiation are not observed in the ectodermal differentiation. Moreover, the expression of ectodermal and endodermal markers at the early differentiation stage is not affected by BAPTA-AM at a concentration affecting the expression of mesodermal and mesendodermal markers in both control and siIP_3R3 cells (Figure 8e). Thus, the apoptosis regulated by IP_3R3 through the alteration of Ca^{2+} signals may not occur in the cells expressing these markers. Taken together, these observations suggest a specific function of IP_3R3 in the regulation of mesodermal and mesendodermal differentiation.

In conclusion, our findings for the first time show that IP_3R3 negatively regulates apoptosis by the alteration of Ca^{2+} oscillation patterns during early mES differentiation. Such effects at least partially contribute to the subsequent mesodermal and mesendodermal differentiation. These findings suggest that a proper apoptotic process during ES cell differentiation is critical for the cell lineage commitment and IP_3R3 might be one of these important regulators. The precise regulation of IP_3R3 and its signaling pathways related to the apoptosis and lineage-specific differentiation of ES cells remains to be elucidated.

Materials and Methods

ES cell culture, *in vitro* differentiation, and transfection. Undifferentiated R1 ES cells were maintained on mitomycin C-inactivated mouse embryonic fibroblast (MEF) feeder layers in the presence of LIF as described earlier.[46] For spontaneous differentiation of ES cells, trypsinized cells were plated on gelatin-coated culture dishes for 30 min to remove MEFs and then non-adherent cells consisting mainly of ES cells were re-placed onto gelatin-coated 35-mm culture dishes at a density of 2000 cells/cm^2 and cultivated in ES cell basic medium without LIF and feeder layers.

Differentiation of mES cells into visceral endodermal cells, cardiomyocytes, chondrocytes, adipocytes, and neurons was initiated by a hanging drop technique as described earlier.[47] Briefly, ESCs were trypsinized and cultivated as EBs using a hanging drop method in the absence of LIF for 2 days, followed by a 5-day suspension cultivation. Then EBs were plated onto gelatin-coated tissue culture dishes. Differentiated visceral endoderm cells with the characteristics of columnar morphology appeared on the periphery of EBs.[48,49] Cardiomyocytes appeared in the form of spontaneously contracting cell clusters and chondrogenic differentiation was detected by Alcian blue staining. For optimal adipogenic differentiation, day 8 EBs were plated on gelatin-coated dishes and cultured with combinations of the following supplements: dexamethasone (10 μm)/β-glycerophosphate (10 mM)/ascorbic acid (50 μg/ml), insulin (85 nM)/triiodothyronine (2 nM) as described earlier.[50] Neuronal differentiation of ES cells was induced based on the method described earlier.[51] EBs were formed in hanging drop for 2 days, followed by a 6-day suspension cultivation. All-*trans* retinoic acid (Sigma, St. Louis, MO, USA) was added during the last 4 days of suspension culture. The 8-day EBs were dissociated into a single cell and then plated onto gelatin-coated over slips in neuronal basal medium (modified MEM containing 10% F12, 2% B27, 1% N2, and 100 mg/ml bovine serum albumin) for further 4–8 days cultivation. All cultivation medium and other substances or cell culture were from Invitrogen-Gibco (Carlsbad, CA, USA) except where indicated.

For transient transfection, R1 ES cells were plated at a density of 3×10^5 cells/35-mm diameter well after 3–5 h of culture and transfected using the Lipofectamine 2000 reagent (Invitrogen) according to the manufacturer's instructions (six-well plates). The apoptotic rate was evaluated with flow cytometry at 72 h after transfection.

RNA interference and overexpression. To make double-stranded siRNA vectors specific for IP_3R3, two independent 19 bp sequences (siIP_3R3a, 5′-TgTCCAg CTTTCTTCACAT-3′ and 5′-ATgTgAAgAAAgCTggACA-3′, and siIP_3R3b, 5′-CTgCAA CACCAgCTggAAg-3′ and 5′-CTTCCAgCTggTgTTgCAg-3′)[38] were cloned into the $pTER^+$ vector.[52] Control siRNA vector was made by selecting 19 bp sequences in the coding region of *EGFP* gene (5′-GGCTACGTCCAGGAGCGCA-3′).[53] The R1 ES cells were transfected with siIP_3R3a or siEGFP plasmids by electroporation, and selected by zeocin (Invitrogen) 30 μg/ml. Single clones were picked and amplified.

For IP_3R3-overexpression experiment, the full-length IP_3R3 (rat) cDNA in $pCB6+$ (IP_3R3wt) was obtained from Dr. GI Bell. The vector pCB6 was used as a control in the experiment.

Immunocytochemical staining. ALP activity was determined by staining using an ALP substrate kit III (Vector Laboratories, Burlingame, CA, USA) according to the manufacturer's instructions. Cells were stained with the primary antibody against SSEA1 (1 : 1000, MC-480, ebioscience, San Diego, CA, USA), α-sarcomeric actinin (1 : 200, Sigma, St Louis, MO, USA), MLC-2v (1 : 50, Alexis, San Diego, CA, USA), Tuj1 (1 : 1000, Promega, Madison, WI, USA), MAP-2 (1 : 100, Chemicon, Billerica, MA, USA), AFP (1 : 1000, Santa Cruz Biotechnology, Santa Cruz, CA, USA), or Dab-2 (1 : 1000, BD Biosciences, Bedford, MA, USA). Rhodamine-conjugated anti-mouse immunoglobulin G antibody (1 : 200, Santa Cruz Biotechnology) was used as a secondary antibody. Primary antibodies were omitted in negative controls. Cells were imaged by using a Leica TCS SP2 confocal laser scanning microscope with $\times 40 - \times 200$ magnification (Leica, Allendale, NJ, USA).

Cell viability proliferation and cell cycle analysis. Cell viability was assessed by 3-(4,5-dimethylthiazol-2-yl)-2,5-diphenyltetrazolium- bromide (MTT) reduction. ES cells were plated at 1000 cells per well in 96-well plates and cultured for 6 days in the presence or absence of LIF and feeder cells. At the indicated times, 20 μl of 5 mg/ml MTT was added, and the cells were incubated for 4 h in a CO_2 incubator. The reagent was reduced by living cells to form an insoluble blue formazan product. After the incubation period, cells were washed with PBS, solubilized with DMSO, and quantified using an enzyme-linked immunosorbent assay reader at the absorbance of 570 nm.

Cell proliferation was determined by measuring the incorporation of BrdU. ES cells were spread without feeder cells and grown in ES cell medium with 100 μM BrdU (Sigma-Aldrich, St Louis, MO, USA) for 30 min. BrdU incorporation was detected by a fluorescence microscope or flow cytometry using an anti-BrdU FITC-conjugated (Becton Dickinson, San Jose, CA, USA) monoclonal antibody. For cell cycle analysis, asynchronously growing ES cells were fixed with ethanol and stained with 50 μg/ml PI containing 0.1 mg/ml RNase A (both from Sigma-Aldrich).[54] Cells were analyzed by flow cytometry to determine G1, S, and G2/M cell cycle distribution (FACStar Plus Flow Cytometer, Becton-Dickinson).

Apoptosis assays. Annexin V staining was used to define the early levels of apoptosis for each ES cell clone. Undifferentiated ES cells and differentiating ES cells at day 3 were harvested and stained with FITC-labeled Annexin V (Annexin V-FITC, BD Biosciences) for flow cytometric analysis. Cells were trypsinized and single-cell suspensions (10^5 cells/clone) were stained with 0.5 μg/ml PI and Annexin V-FITC (dilution 1 : 20) according to the manufacturer's instructions.

TUNEL staining was performed with the *in situ* Cell Death Detection kit (Roche Diagnostics, Mannheim, Germany). Differentiating ES cells were fixed and incubated with TUNEL reaction mixture according to the manufacturer's instructions. The TUNEL signal was detected by a microscope and flow cytometric analysis separately.

Measurement of caspase-3 activity. Caspase-3 activity was measured using the CaspACETM colorimetric assay system (Promega) according to the manufacturer's instructions. Briefly, cells were harvested and resuspended in cell lysis buffer (2×10^7/ml) on differentiation day 3. Lysates were centrifuged (16 000 $\times$ *g*) for 10 min at 4 °C. Then, 10 μl of supernatant was mixed with 80 μl of assay buffer and 10 μl of 2 mM Asp-Glu-Val-Aspp-nitroanilide substrate. After incubation at 37 °C for 2–4 h, absorbance was measured using a microplate reader at 405 nm. The absorbance of each sample was determined by subtracting the mean absorbance of the blank from that of the sample.

Ca^{2+} imaging. Cells were loaded with 2 μM of Flue4-AM (Molecular Probes, Eugene, OR, USA) for 15 min at 37 °C, and then de-esterification of the dye was allowed for another 15 min.[24] Ca^{2+} imaging was performed using a Leica TCS SP2 confocal laser scanning microscope with appropriate fluorescence filters at room temperature. Data are expressed as F/F_0, where F is the absolute fluorescence value in an area of interest and F_0 is the resting fluorescence recorded under steady-state conditions. Confocal whole cell images were taken at a time interval of 5 s.

Reverse transcription (RT)-PCR. Total RNA was extracted from the cells using TRIzol (Invitrogen) and transcribed into cDNA using oligo (dT) and ReverTra Ace reverse transcriptase (Toyobo, Osaka, Japan). The PCR primers are listed in Table 1 and Supplementary Table 1. Samples were amplified in the linear range by PCR. The PCR products were size-fractionated by 1–1.5% agarose gel containing ethidium bromide.

Quantitative RT-PCR (Q-PCR). Total RNA was extracted from cells and analyzed by kinetic real-time PCR using the ABI PRISM 7900 system (Applied Biosystems, Foster City, CA, USA) with SYBR Green PCR core reagents (Applied Biosystems) for relative quantification of the indicated genes. The transcript of glyceraldehyde 3-phosphate dehydrogenase (GADPH) was used for internal normalization. The Q-PCR primers are listed in Table 2.

Immunoblot analysis. The cells were lysed in a ice-cold lysis buffer containing 50 mM Tris-Cl, pH 7.5, 100 mM NaCl, 1 mM EDTA, 1% TritonX-100, 1 mM PMSF, 1 μg/ml leupeptin, and 1 μ/ml pepstain A. The protein concentration in the supernatant was determined using a BCA protein assay (Pierce, Rockford, IL, USA). Samples were subjected to 8–12% SDS-polyacrylamide gel electrophoresis, and the separated proteins were electrophoretically transferred to polyvinylindene difluoride membranes (Bio-Rad, Hercules, CA, USA). Blots were incubated with the primary antibody against Oct-4 (1 : 1000, a kind gift from Dr. Ying Jin), β-actin (1 : 3000, Sigma), IP_3R1 (1 : 1000, Upstate, Lake Placid, NY, USA), IP_3R2 (1 : 1000, Chemicon), IP_3R3 (1 : 1000, BD Biosciences), Bax (1 : 1000, Cell Signaling Technology, Beverly, MA, USA), caspase-3 (1 : 1000, Cell Signaling Technology), or cytochrome *c* (1 : 1000, Santa Cruz Biotechnology). The membranes were then incubated with horseradish peroxidase-linked secondary anti-rabbit (Santa Cruz Biotechnology) or anti-mouse antibodies (Sigma). The immunoreaction was visualized with a chemiluminescent kit (Perkin-Elmer Life Sciences, Waltham, MA, USA).

Flow cytometry analysis. Cells (10^5) were washed with PBS and resuspended in 1-ml PBS, which contained anti-Flk-1 antibody (1 : 200, eBioscience), placed on ice for 30 min, followed by a single wash with 10 ml PBS. Phycoerythrin (PE)-conjugated anti-mouse immunoglobulin G antibody (1 : 1000, BD Biosciences) was used as a secondary antibody. Cells were analyzed by flow cytometry (FACStar Plus Flow Cytometer, Becton-Dickinson).

Statistical analysis. Data are expressed as mean $\pm$ S.E.M. The statistical significance of differences was estimated by one-way ANOVA or Student's *t*-test, when appropriate (SPSS 13.0 software, SPSS Inc. Chicago, IL, USA). $P < 0.05$ was considered significant.

Table 1 Primer sequences for RT-PCR

Gene	Primer sequence (5′to 3′)	AT (°C)	PS (bp)
IP3R1	5′-CTGGGAGCTTTCAATGTCTGC-3′ 5′-GCAGTTCTCCCCCGTCTCTAC-3′	61	446
IP3R2	5′-GGCTCGGTCAATGGCTTC-3′ 5′-CCCCTGTTTCGCCTGCTT-3′	60	183
IP3R3	5′-AGAACGACCGCAGGTTTG-3′ 5′-CCCTTGTCACGGAATGGA-3′	61	193
Nanog	5′-CCCCAGGGCTATCTGGTGAAC-3′ 5′-AAGTTTTGCTGCAACTGTACGT-3′	55	220
Mef2c	5′-AGATACCCACAACACACCACGCG CC-3′ 5′-CATTATCCTTCAGAGAGTCGCATGC GCTT-3′	59	195
Nkx2.5	5′-GCCAACAGCAACTTCGTGA-3′ 5′-CCGGTCCTAGTGTGGAATC-3′	59	350
αMHC	5′-GCGCATCAAGGAGCTCAC-3′ 5′-GGAACTTGGACAGGTTGGTG-3′	59	155
Mlc-2v	5′-TGTGGGTCACCTGAGGCTGTGGT TCAG-3′ 5′-GAAGGCTGACTATGTCCGGGAGA TGC-3′	60	190
CK8	5′-CCTAATCCTCTGGCCAACCT-3′ 5′-ACTGAATTGGGTTTGGATGG-3′	59	84
HNF3β	5′-GGGAAATGAGAGGCTGAGTG-3′ 5′-GGTGAGACTGCTCCCTTGAG-3′	59	81
AIB1	5′-TCAGGACTCATCTTTTCTGTTGG-3′ 5′-GCAGCACAGAGACAAGAAGTCA-3′	59	88
AFP	5′-ATTCCTCCCAGTGCGTGAC-3′ 5′-CAGCAGCCTGAGAGTCCAT-3′	59	230
Dab2	5′-GGCAACAGGCTGAACCATTAGT-3′ 5′-TTGGTGTCGATTTCAGAGTTTAGAT-3′	59	300
sdc4	5′-GGGCAAGAAACCCATCTACAAA-3′ 5′-CTCCACTCCTCTCCCCAATAAGT-3′	59	78
tmpress2	5′-CCAGCCCAGTACTACCCATCTC-3′ 5′-GCTCCTGAGGACTTGGGATGT-3′	59	80
m28s	5′-AGCAGCCGACTTAGAACTGG-3′ 5′-TAGGGACAGTGGGAATCTCG-3′	55	250

AT, annealing temperature; PS, product size.

Table 2 Primer sequences for RT-PCR

Gene	Primer sequence (5′to 3′)	AT (°C)	PS (bp)
Oct-4	5′-TCAGCTTGGGCTAGAGAAGG-3′ 5′-TGACGGGAACAGAGGGAAAG-3′	59	254
Rex1	5′-AGCAGGATCGCCTCACTG-3′ 5′-GGCCACTTGTCTTTGCCG-3′	59	188
Fgf-5	5′-GGGCATCGGTTTCCATC-3′ 5′-CTCCCTGAACTTACAGTCATCC-3′	59	207
Nestin	5′-TGAGGGTCAGGTGGTTCTG-3′ 5′-AGAGCAGGGAGGGACATTC-3′	59	230
Gata4	5′-CCTGGAAGACACCCCAATCTC-3′ 5′-AGGTAGTGTCCCGTCCCATCT-3′	59	116
Gata6	5′-GCTGAACGGAACGTACCACC-3′ 5′-ACAGTGGCGTCTGGATGGAG-3′	59	230
Brachyury	5′-CCACCGCTGGAAATATGTG-3′ 5′-CAGCTATGAACTGGGTCTCG-3′	59	286
Flk1	5′-CTGTGGCGTTTCCTACTCCT-3′ 5′-AGGAGCAAGCTGCATCATTT-3′	59	92
Gsc	5′-GCAAGGACTTGCACAGACAG-3′ 5′-CAGCTAGCTCCTCGTTGCTT-3′	59	84
Hand1	5′-TCGGCAGGTCCTTCGTGT-3′ 5′-GCTGTCAGCCCAATTAGCA-3′	59	136
GAPDH	5′-GTGGCAAAGTGGAGATTGTTG-3′ 5′-CTCCTGGAAGATGGTGATGG-3′	59	163

AT, annealing temperature; PS, product size.

Conflict of interest

The authors declare no conflict of interest.

Acknowledgements. This study was supported by grants from the State Major Research Program of China (No. 2006CB0F0900, No. 2007CB947900), National Science Foundation of China (30671045), and Knowledge Innovation Program of CAS (KSCX2-YW-R-233). We thank Drs. Hans Clevers and Marc van de Wetering for sharing their pTER + plasmid with us, Dr. GI Bell for providing pCB6 + and pCB6-(rat) IP_3R3 vectors, and Dr. Yu-Fang Shi for kindly providing the adipogenic reagents.

1. Evans MJ, Kaufman MH. Establishment in culture of pluripotential cells from mouse embryos. *Nature* 1981; **292**: 154–156.
2. Thomson JA, Itskovitz-Eldor J, Shapiro SS, Waknitz MA, Swiergiel JJ, Marshall VS *et al.* Embryonic stem cell lines derived from human blastocysts. *Science* 1998; **282**: 1145–1147.
3. Nagy A, Rossant J, Nagy R, Bramow-Newerly W, Roder JC. Derivation of completely cell culture-derived mice from early-passage embryonic stem cells. *Proc Natl Acad Sci USA* 1993; **90**: 8424–8428.
4. Duval D, Reinhardt B, Kedinger C, Boeuf H. Role of suppressors of cytokine signaling (Socs) in leukemia inhibitory factor (LIF) -dependent embryonic stem cell survival. *FASEB J* 2000; **14**: 1577–1584.
5. Duval D, Malaise M, Reinhardt B, Kedinger C, Boeuf H. A p38 inhibitor allows to dissociate differentiation and apoptotic processes triggered upon LIF withdrawal in mouse embryonic stem cells. *Cell Death Differ* 2004; **11**: 331–341.
6. Jacobson MD, Weil M, Raff MC. Programmed cell death in animal development. *Cell* 1997; **88**: 347–354.
7. Boheler KR, Czyz J, Tweedie D, Yang HT, Anisimov SV, Wobus AM. Differentiation of pluripotent embryonic stem cells into cardiomyocytes. *Circ Res* 2002; **91**: 189–201.
8. Berridge MJ, Lipp P, Bootman MD. The versatility and universality of calcium signalling. *Nat Rev Mol Cell Biol* 2000; **1**: 11–21.
9. Berridge MJ, Bootman MD, Roderick HL. Calcium signalling: dynamics, homeostasis and remodelling. *Nat Rev Mol Cell Biol* 2003; **4**: 517–529.
10. Stachecki JJ, Armant DR. Transient release of calcium from inositol 1,4,5-trisphosphate-specific stores regulates mouse preimplantation development. *Development* 1996; **122**: 2485–2496.
11. Kume S, Muto A, Inoue T, Suga K, Okano H, Mikoshiba K. Role of inositol 1,4,5-trisphosphate receptor in ventral signaling in Xenopus embryos. *Science* 1997; **278**: 1940–1943.
12. Ashworth R, Devogelaere B, Fabes J, Tunwell RE, Koh KR, De SH *et al.* Molecular and functional characterization of inositol trisphosphate receptors during early zebrafish development. *J Biol Chem* 2007; **282**: 13984–13993.
13. Khan AA, Soloski MJ, Sharp AH, Schilling G, Sabatini DM, Li SH *et al.* Lymphocyte apoptosis: mediation by increased type 3 inositol 1,4,5-trisphosphate receptor. *Science* 1996; **273**: 503–507.
14. Duval D, Trouillas M, Thibault C, Dembele D, Diemunsch F, Reinhardt B *et al.* Apoptosis and differentiation commitment: novel insights revealed by gene profiling studies in mouse embryonic stem cells. *Cell Death Differ* 2006; **13**: 564–575.
15. Mendes CC, Gomes DA, Thompson M, Souto NC, Goes TS, Goes AM *et al.* The type III inositol 1,4,5-trisphosphate receptor preferentially transmits apoptotic Ca2+ signals into mitochondria. *J Biol Chem* 2005; **280**: 40892–40900.
16. White C, Li C, Yang J, Petrenko NB, Madesh M, Thompson CB *et al.* The endoplasmic reticulum gateway to apoptosis by Bcl-X(L) modulation of the InsP3R. *Nat Cell Biol* 2005; **7**: 1021–1028.
17. Li C, Wang X, Vais H, Thompson CB, Foskett JK, White C. Apoptosis regulation by Bcl-x(L) modulation of mammalian inositol 1,4,5-trisphosphate receptor channel isoform gating. *Proc Natl Acad Sci USA* 2007; **104**: 12565–12570.
18. Patel S, Patel S, Joseph SK, Joseph SK, Thomas AP, Thomas AP. Molecular properties of inositol 1,4,5-trisphosphate receptors. *Cell Calcium* 1999; **25**: 247–264.
19. Taylor CW, Genazzani AA, Morris SA. Expression of inositol trisphosphate receptors. *Cell Calcium* 1999; **26**: 237–251.
20. Furuichi T, Simon-Chazottes D, Fujino I, Yamada N, Hasegawa M, Miyawaki A *et al.* Widespread expression of inositol 1,4,5-trisphosphate receptor type 1 gene (Insp3r1) in the mouse central nervous system. *Receptors Channels* 1993; **1**: 11–24.
21. Matsumoto M, Nakagawa T, Inoue T, Nagata E, Tanaka K, Takano H *et al.* Ataxia and epileptic seizures in mice lacking type 1 inositol 1,4,5-trisphosphate receptor. *Nature* 1996; **379**: 168–171.
22. Matsumoto M, Nagata E. Type 1 inositol 1,4,5-trisphosphate receptor knock-out mice: their phenotypes and their meaning in neuroscience and clinical practice. *J Mol Med* 1999; **77**: 406–411.
23. Yanagida E, Shoji S, Hirayama Y, Yoshikawa F, Otsu K, Uematsu H *et al.* Functional expression of Ca2+ signaling pathways in mouse embryonic stem cells. *Cell Calcium* 2004; **36**: 135–146.
24. Kapur N, Mignery GA, Banach K. Cell cycle-dependent calcium oscillations in mouse embryonic stem cells. *Am J Physiol Cell Physiol* 2007; **292**: C1510–C1518.
25. Rizzuto R, Pinton P, Ferrari D, Chami M, Szabadkai G, Magalhaes PJ *et al.* Calcium and apoptosis: facts and hypotheses. *Oncogene* 2003; **22**: 8619–8627.
26. Lubitz S, Glaser S, Schaft J, Stewart AF, Anastassiadis K. Increased apoptosis and skewed differentiation in mouse embryonic stem cells lacking the histone methyltransferase Mll2. *Mol Biol Cell* 2007; **18**: 2356–2366.
27. Ismailoglu I, Yeamans G, Daley GQ, Perlingeiro RC, Kyba M. Mesodermal patterning activity of SCL. *Exp Hematol* 2008; **36**: 1593–1603.
28. Bi W, Deng JM, Zhang Z, Behringer RR, de CB. Sox9 is required for cartilage formation. *Nat Genet* 1999; **22**: 85–89.
29. Kosher RA, Kulyk WM, Gay SW. Collagen gene expression during limb cartilage differentiation. *J Cell Biol* 1986; **102**: 1151–1156.
30. Tashiro K, Inamura M, Kawabata K, Sakurai F, Yamanishi K, Hayakawa T *et al.* Efficient adipocyte and osteoblast differentiation from mouse induced pluripotent stem cells by adenoviral transduction. *Stem Cells* 2009; **27**: 1802–1811.
31. Couchman JR, Woods A. Syndecan-4 and integrins: combinatorial signaling in cell adhesion. *J Cell Sci* 1999; **112** (Part 20): 3415–3420.
32. Vaarala MH, Porvari KS, Kellokumpu S, Kyllonen AP, Vihko PT. Expression of transmembrane serine protease TMPRSS2 in mouse and human tissues. *J Pathol* 2001; **193**: 134–140.
33. Yang DH, Cai KQ, Roland IH, Smith ER, Xu XX. Disabled-2 is an epithelial surface positioning gene. *J Biol Chem* 2007; **282**: 13114–13122.
34. Miwa K, Lee JK, Hidaka K, Shi RQ, Morisaki T, Kodama I. Optimal population of embryonic stem cells in 'Hanging drop' culture for *in-vitro* differentiation to cardiac myocytes. *Environ Med* 2002; **46**: 92–94.
35. Berridge MJ. Elementary and global aspects of calcium signalling. *J Physiol* 1997; **499** (Part 2): 291–306.
36. Fu JD, Yu HM, Wang R, Liang J, Yang HT. Developmental regulation of intracellular calcium transients during cardiomyocyte differentiation of mouse embryonic stem cells. *Acta Pharmacol Sin* 2006; **27**: 901–910.
37. Khan MT, Bhanumathy CD, Schug ZT, Joseph SK. Role of inositol 1,4,5-trisphosphate receptors in apoptosis in DT40 lymphocytes. *J Biol Chem* 2007; **282**: 32983–32990.
38. Hattori M, Suzuki AZ, Higo T, Miyauchi H, Michikawa T, Nakamura T *et al.* Distinct roles of inositol 1,4,5-trisphosphate receptor types 1 and 3 in Ca^{2+} signaling. *J Biol Chem* 2004; **279**: 11967–11975.
39. Hagar RE, Burgstahler AD, Nathanson MH, Ehrlich BE. Type III InsP3 receptor channel stays open in the presence of increased calcium. *Nature* 1998; **396**: 81–84.
40. Bezprozvanny I, Watras J, Ehrlich BE. Bell-shaped calcium-response curves of Ins(1,4,5)P3- and calcium-gated channels from endoplasmic reticulum of cerebellum. *Nature* 1991; **351**: 751–754.
41. Mak DO, McBride S, Foskett JK. Regulation by Ca^{2+} and inositol 1,4,5-trisphosphate (InsP3) of single recombinant type 3 InsP3 receptor channels. Ca^{2+} activation uniquely distinguishes types 1 and 3 insp3 receptors. *J Gen Physiol* 2001; **117**: 435–446.
42. Boulay G, Brown DM, Qin N, Jiang M, Dietrich A, Zhu MX *et al.* Modulation of Ca(2+) entry by polypeptides of the inositol 1,4, 5-trisphosphate receptor (IP3R) that bind transient receptor potential (TRP): evidence for roles of TRP and IP3R in store depletion-activated Ca(2+) entry. *Proc Natl Acad Sci USA* 1999; **96**: 14955–14960.
43. Zhong F, Davis MC, McColl KS, Distelhorst CW. Bcl-2 differentially regulates Ca^{2+} signals according to the strength of T cell receptor activation. *J Cell Biol* 2006; **172**: 127–137.
44. Blackshaw S, Sawa A, Sharp AH, Ross CA, Snyder SH, Khan AA. Type 3 inositol 1,4,5-trisphosphate receptor modulates cell death. *FASEB J* 2000; **14**: 1375–1379.
45. Yasunaga M, Tada S, Torikai-Nishikawa S, Nakano Y, Okada M, Jakt LM *et al.* Induction and monitoring of definitive and visceral endoderm differentiation of mouse ES cells. *Nat Biotechnol* 2005; **23**: 1542–1550.
46. Fu JD, Li J, Tweedie D, Yu HM, Chen L, Wang R *et al.* Crucial role of the sarcoplasmic reticulum in the developmental regulation of Ca^{2+} transients and contraction in cardiomyocytes derived from embryonic stem cells. *FASEB J* 2006; **20**: 181–183.
47. Wobus AM, Guan K, Yang HT, Boheler KR. Embryonic stem cells as a model to study cardiac, skeletal muscle, and vascular smooth muscle cell differentiation. *Methods Mol Biol* 2002; **185**: 127–156.
48. Murray P, Edgar D. The regulation of embryonic stem cell differentiation by leukaemia inhibitory factor (LIF). *Differentiation* 2001; **68**: 227–234.
49. O'Shea KS. Self-renewal vs differentiation of mouse embryonic stem cells. *Biol Reprod* 2004; **71**: 1755–1765.
50. Kawaguchi J, Mee PJ, Smith AG. Osteogenic and chondrogenic differentiation of embryonic stem cells in response to specific growth factors. *Bone* 2005; **36**: 758–769.
51. Bain G, Kitchens D, Yao M, Huettner JE, Gottlieb DI. Embryonic stem cells express neuronal properties *in vitro*. *Dev Biol* 1995; **168**: 342–357.
52. van de WM, Oving I, Muncan V, Pon Fong MT, Brantjes H, van LD *et al.* Specific inhibition of gene expression using a stably integrated, inducible small-interfering-RNA vector. *EMBO Rep* 2003; **4**: 609–615.
53. Wang BB, Lu R, Wang WC, Jin Y. Inducible and reversible suppression of Npm1 gene expression using stably integrated small interfering RNA vector in mouse embryonic stem cells. *Biochem Biophys Res Commun* 2006; **347**: 1129–1137.
54. Yang WW, Wang ZH, Zhu Y, Yang HT. E2F6 negatively regulates ultraviolet-induced apoptosis via modulation of BRCA1. *Cell Death Differ* 2007; **14**: 807–817.

Supplementary Information accompanies the paper on Cell Death and Differentiation website (http://www.nature.com/cdd)